New evidence for an ENSO impact on low-latitude glaciers: Antizana 15, Andes of Ecuador, 0°28′S

Bernard Francou,[1] Mathias Vuille,[2] Vincent Favier,[3] and Bolivar Cáceres[4]

Received 22 December 2003; revised 3 June 2004; accepted 8 June 2004; published 17 September 2004.

[1] Continuous monthly mass balance measurements from the ablation zone of Antizana 15 glacier in the Andes of Ecuador between January 1995 and December 2002 indicate a strong dependence on El Niño–Southern Oscillation (ENSO). Over the 8-year period investigated, mass balance was negative all year round during El Niño periods but remained close to equilibrium (positive anomalies) during La Niña events. On seasonal timescales, mean ablation rates remain at a quite constant level all year round, but interannual variability shows much larger changes from year to year during the key periods February–May and September. This variability is caused by large differences that occur in the seasonal cycle during the two opposite phases of ENSO. Since ENSO is phase locked to the seasonal cycle with largest sea surface temperature anomalies around boreal winter, November–February, and the atmospheric response to ENSO is delayed by 3 months over the Ecuadorian Andes, year-to-year variations in mass balance are largest between February and May. Energy balance studies at the glacier surface indicate that high air temperature, which favors rain over snowfall, weak and sporadic snowfall, insufficient to maintain a high glacier albedo, low wind speeds, which limit the transfer of energy from melting to sublimation, and reduced cloud cover, which increases the incoming short-wave radiation, are the dominant factors related to El Niño, which tend to increase ablation. La Niña events on the other hand are characterized by colder temperatures, higher snowfall amounts, and to a lesser degree, more constant winds, factors which increase albedo and sublimation and therefore preclude melting at the glacier surface. The effects of ENSO variability are also important over the accumulation area, which represents up to 80% of the glacier surface during La Niña events (1999–2000) and 45–60% in El Niño years. Since the accumulation rates increase during these cold periods, the specific net balance and the dynamics of the entire glacier are strongly affected. Longer mass balance records than this 8-year period are needed for conclusive answers about the dependence of the Ecuadorian glaciers on ENSO variability, but initial results suggest that the response observed on Antizana glaciers is very similar to what has been observed previously during ENSO periods on Andean glaciers in the outer tropics. The seasonal dependence on ENSO and the physical mechanisms linking ENSO with mass balance variations on Antizana, however, are different from the response observed on Andean glaciers in the outer tropics. *INDEX TERMS:* 1620 Global Change: Climate dynamics (3309); 1827 Hydrology: Glaciology (1863); 1863 Hydrology: Snow and ice (1827); 3374 Meteorology and Atmospheric Dynamics: Tropical meteorology; 4522 Oceanography: Physical: El Nino; *KEYWORDS:* tropical glacier, ENSO, mass balance

Citation: Francou, B., M. Vuille, V. Favier, and B. Cáceres (2004), New evidence for an ENSO impact on low-latitude glaciers: Antizana 15, Andes of Ecuador, 0°28′S, *J. Geophys. Res.*, *109*, D18106, doi:10.1029/2003JD004484.

1. Introduction

[2] Studies on glacier retreat and mass balance variability in the tropical and subtropical Andes have gained considerable attention over the past few years, primarily because of the growing awareness that many of these glaciers are retreating at an increasing pace since the late 1970s. Early studies focusing on interannual mass balance variations on glaciers in Bolivia noted that years with a negative mass balance tend to coincide with warm El Niño–Southern Oscillation (ENSO) events in the Pacific [*Francou et al.*, 1995a, 1995b; *Ribstein et al.*, 1995]. On the basis of these

[1]Laboratoire de Glaciologie et de Géophysique de l'Environnement (LGGE), Institut de Recherche pour le Developpement (IRD), Saint Martin d'Hères, France.
[2]Climate System Research Center, Department of Geosciences, University of Massachusetts, Amherst, Massachusetts, USA.
[3]Maison des Sciences de l'Eau, Institut de Recherche pour le Developpement, Montpellier, France.
[4]Instituto Nacional de Meteorología e Hidrología (INAMHI), Quito, Ecuador.

0148-0227/04/2003JD004484$09.00

early studies it was hypothesized that the accelerated glacier retreat in this region may be linked to an increased frequency and intensity of El Niño events over the last three decades. More recent studies emphasized the physical processes at the glacier surface based on energy balance measurements on Zongo glacier (Bolivia) during contrasting years such as the exceptional 1997–1998 warm ENSO phase and the preceding moderate 1996–1997 ENSO cold phase [*Wagnon et al.*, 2001] or investigated the mechanisms linking the ENSO-related large-scale atmospheric dynamics with mass balance variations in the subtropical Andes [*Francou et al.*, 2003]. These glaciological studies come in support of climatological evidence indicating that a large fraction of interannual climate variability in the central (subtropical) Andes is associated with ENSO [e.g., *Aceituno and Montecinos*, 1993; *Vuille*, 1999; *Vuille et al.*, 2000a; *Garreaud and Aceituno*, 2001; *Garreaud et al.*, 2003; *Vuille et al.*, 2003]. For instance, in Bolivia (16°S), ENSO events often lead to a significant change in the amount of precipitation falling during the austral summer wet season (wet anomalies during La Niña and dry anomalies during El Niño years) but also exhibit a marked temperature anomaly (cold anomalies during La Niña and warm anomalies during El Niño years) [*Vuille*, 1999; *Vuille and Bradley*, 2000]. The impact of ENSO events on subtropical glacier mass balance is further enhanced by the fact that ENSO is phase locked to the seasonal cycle and tends to peak during the austral summer months October–April, which control more than 90% of the interannual mass balance variance [*Francou et al.*, 2003]. As shown by *Wagnon et al.* [1999, 2001], the main factor governing melting is precipitation, which is mainly solid at the elevation of glacier snouts, and, in consequence, it has an important feedback on the net radiation balance via the albedo. Air temperature, on the other hand, does not have a strong direct impact on melting because the radiative fluxes and the atmospheric humidity are more important factors of the energy balance than the sensible heat flux and because the snow/rain limit usually lies below the glacier snout even during warm ENSO years [*Wagnon et al.*, 1999; *Sicart*, 2002].

[3] In June 1994 the network of monitored glaciers was extended to the Antizana 15 glacier in the inner tropical Andes of Ecuador, marked by only minor seasonal variations. This extension now permits a comparison with the glacier evolution in the subtropical or so-called outer tropical Andes [*Kaser and Osmaston*, 2002] of Bolivia and southern Peru, where both precipitation and temperature feature a distinct seasonality. For the last 8 years, permanent specific net balance observations have been collected on Antizana. Mass balance surveys have been conducted every month in the ablation area, i.e., at the 5100–4800 m above sea level (asl) elevation range, thereby offering new year-round insight into the spatiotemporal mass balance variability of the ablation zone [*Francou et al.*, 2000]. Antizana 15 is located on the Amazonian slope of the Andes, 300 km east from the Pacific coast, which usually records strong local sea surface temperature anomalies (SSTA) during ENSO events (Niño 1 + 2 region). Several recent studies have discussed the significant changes in precipitation, cloud cover, and temperature that occur during ENSO all along the Pacific coast and the western slope of the Ecuadorian Andes [*Rossel et al.*, 1998; *Bendix*, 2000; *Vuille et al.*, 2000b; *Bendix et al.*, 2003]. The northeastern cordillera equally experiences significant temperature changes during ENSO periods, but precipitation anomalies during El Niño/La Niña years do not seem to be as pronounced as along the coast or in the northwestern Ecuadorian Andes [*Vuille et al.*, 2000b]. A preliminary study on Antizana glacier revealed that ablation rates systematically increase during Pacific warm events and decrease during cold periods and that this response is more or less synchronous with equatorial Pacific SSTA [*Francou et al.*, 2000]. How these mass balance variations are linked to the background climate and what physical mechanisms govern the ablation rate, however, has not yet been analyzed.

[4] Here we present a new, continuous, monthly mass balance record from Antizana 15, measured between January 1995 and December 2002. This 96-month period was marked by alternating warm, cold, and neutral ENSO phases. The aim of this study is to compare the mass balance measurements with local climate and large-scale atmospheric dynamics in the tropical Pacific–South America domain. Special consideration will be given to the extreme phases of ENSO and the impact they have had on the measured mass balance. To gain a better understanding of the glacier-climate interactions and the relevant physical processes at the glacier surface, we will also discuss results from a recent energy balance study performed in the ablation zone during a complete annual cycle and then extrapolated over the entire 8 years. This later study is presented in more detail in a companion paper by *Favier et al.* [2004] and will only be discussed here in summarized form, where the results are pertinent to the understanding of the paper.

[5] In section 2 we present the study area and we give a short introduction to the climatic setting. Section 3 includes an overview of data and methods that were used, and section 4 presents mass balance variations on seasonal and interannual timescales. In section 5 we discuss the main terms of the energy balance at the glacier surface, while section 6 focuses on the response of the glacier during extreme phases of ENSO. Section 7 presents the large and mesoscale atmospheric circulation associated with positive and negative mass balance anomalies on Antizana 15. Finally section 8 ends with a summary and some concluding remarks on the value of such a short record and the significance of our conclusions inferred from only 8 years of data.

2. Study Area and Climatic Setting

[6] Antizana glacier 15 (0°28′S, 78°09′W) is one of the 17 glaciers listed in 1975 by *Hastenrath* [1981] on this active volcano located 40 km east of Quito. Facing NW, between 5760 m asl and 4840 m asl, this 1.96-km-long glacier in 2002 covered an area of 0.71 km^2. The summit forms a small ice cap, and the glacier Antizana 15 then follows a steep slope toward its lower part, where, below 5100 m asl, it is divided into two parallel tongues, named 15α (south) and 15β (north) (Figure 1). The extent of the glacier 15 was first documented in the mid-1950s. The surface area was controlled in 1956, 1965, 1993, and 1997 by aerial photogrammetry. Since 1995 a ground topographic survey and a monitoring of pits and stakes located along the tongue α allow an estimate of the annual mass balance of

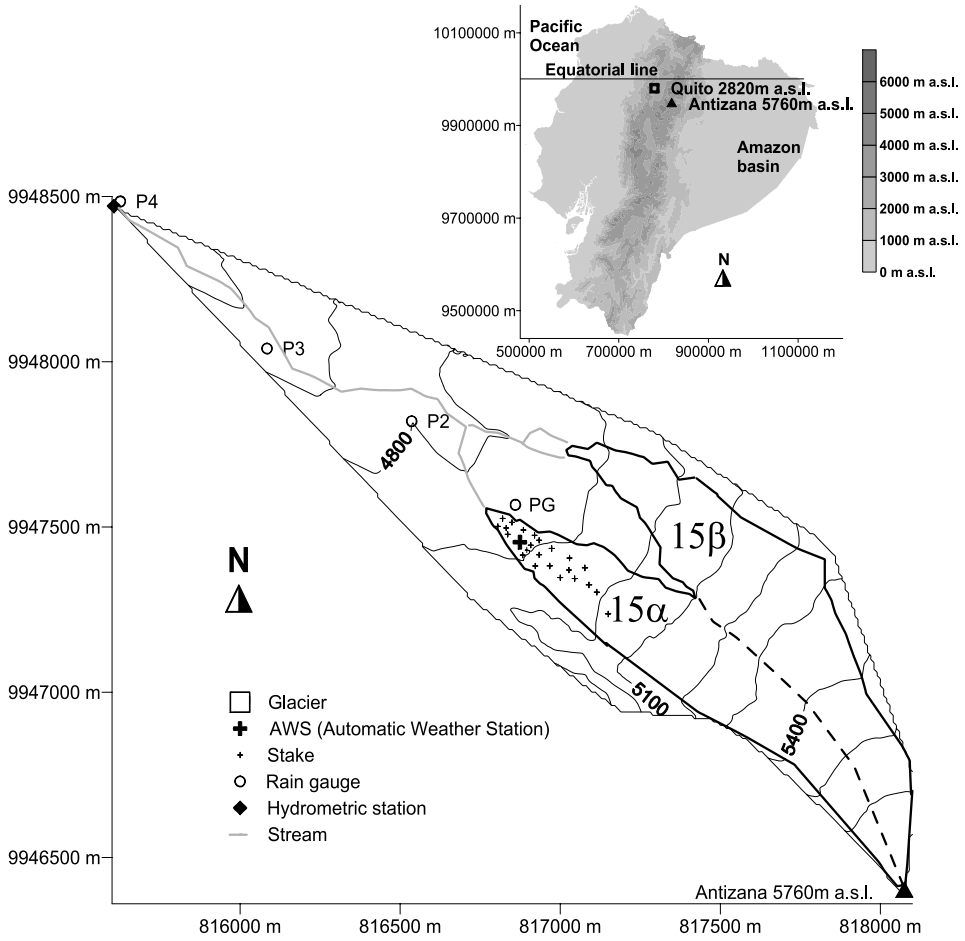

Figure 1. The two glaciers 15 of Antizana, with location of the main equipment installed on or near the glacier. Inset shows location of Antizana glacier within Ecuador. Projection is on universal transverse Mercator zone 17. Glacier is in the limits of December 2002. Several rain gauge sites (PG, P2, P3, and P4) are shown. Dashed line separates glacier tongues 15α and 15β. Solid triangle indicates location of peak of Antizana Volcano (5760 m asl).

the glacier 15α [*Bontron et al.*, 1999; *World Glacier Monitoring Service*, 2003]. From 1956 to 1965 the average deficit of this glacier was estimated to be 251 mm water equivalent (w.e.) yr^{-1}. It was reduced to 146 mm w.e. yr^{-1} during the 1965–1993 period but then accelerated dramatically in the next 5 years, 1993–1998, to reach 600 mm w.e. yr^{-1} [*Francou et al.*, 2000]. Two consecutive positive mass balance years in 1999 and 2000 (515 mm w.e. and 393 mm w.e., respectively) provoked an immediate and significant snout advance of 40-m distance during those two years, which stopped the accelerated retreat of 160 m observed during 1995–1998 [*Cáceres et al.*, 2002]. This behavior suggests that glacier dynamics respond immediately to mass balance changes. Future changes in glacier extent may have major ramifications for Quito, as meltwater from Antizana glaciers provides part of the drinking water supply for Ecuador's largest city and capital.

[7] In this study, only the ablation area of glacier 15α will be considered. This zone extends below 5300 m asl and was within the range of equilibrium line fluctuations during the investigated period. Being permanently surveyed by a dense stake network, the ablation zone represents ~27% of the total area (glacier in equilibrium).

[8] The Antizana area is representative of the Eastern Cordillera by being directly exposed to moist easterly winds from the Amazon basin. Nevertheless, the northwestern slope of glacier 15 lies in a relatively sheltered position with reduced cloud cover, and precipitation does not exceed 1200 mm yr^{-1}. Precipitation falls year-round, with a maximum from February to June. A second period with important precipitation amounts may be observed between September and November. The precipitation cycle does not show a clear dry season since each month receives a minimum of 50 mm w.e. Consistent with precipitation, convective cloudiness also features two clear maximums, one in March, April, and May (MAM), and a smaller one in September, October, and November, interrupted by two minimums in June, July, and August (JJA) and December, January, and February. Temperature is almost constant and does not display any significant seasonal variations, but the interannual variability is large. Wind is the principal factor of seasonality in this part of the Ecuadorian cordillera, and the year can clearly be divided into two parts: a first period, between April and September, where middle and upper tropospheric easterly winds are strong and almost constant, and a second period, from October to March, where winds

are weak and intermittent, particularly between October and January.

3. Data and Methods

3.1. Mass Balance in the Ablation Area

[9] Mass balance was measured by a network of stakes surveyed at the beginning of every month. In June 1994, 14 stakes were inserted into 10-m-deep holes on the central axis of the glacier between 5050 m asl and 4840 m asl. In the following year the network was increased, and stakes were added on the north and south sides of the tongue in order to better capture the spatiotemporal variations of seasonal ablation changes. From then on, a minimum of 20 stakes was regularly surveyed and replaced every year in January and put 20–30 m upstream. Each elevation range of 50 m includes a minimum of four stakes. Snow depth, when present on the ice, was directly measured with an aluminum rod on several points inside a 1-m circle around the stake. Snow density ρ was generally only estimated because of its low variability. Indeed, snowfalls occur during relatively warm conditions (temperature around $-2°$–$0°$C), and the transformation of fresh snow into firn is rapid, leading to an increase in density to values close to $\rho = 400$–450 kg m^{-3} within 1 or 2 days. After this initial densification, snow/firn density evolves slowly. However, whenever the glacier was found with a fresh dry snow cover, or when the firn evolution was estimated to be more complete ($\rho > 500$ kg m^{-3}), the snow density was measured in one or two pits. To process the net specific balance, we divided the ablation zone into elevation ranges of 30–50 m and performed homogeneity tests between all stakes belonging to one elevation range to eliminate nonrepresentative points. To account for changes in surface elevation, new topographic surveys were performed every year at the beginning of the hydrological year using a theodolite with a distanciometer. Because the annual cycle of accumulation at high altitude generally starts in January, the hydrological year in this part of Ecuador was set to coincide with the calendar year from 1 January to 31 December. Thus this study is based on a continuous series of 96 months, from January 1995 to December 2002. During this 8-year period the specific net balance of the entire glacier was also estimated every year by integrating net accumulation measurements performed in the upper glacier zone at the beginning of the hydrological year. This paper does not discuss these data any further, but they allowed reconstructing the dynamics of the entire glacier, and they were used to locate the equilibrium line altitude (ELA) and hence to determine the upper limit of the ablation area.

3.2. Meteorological Data

[10] Precipitation was measured at several locations surrounding the glacier (Figure 1). Since accurate precipitation data are not available in this zone before 1994, several rain gauges were installed between the glacier terminus (PG at 4860 m asl), the moraine of the 1950s (P2 at 4785 m asl), the lower moraine of the Little Ice Age (P3 at 4650 m asl), and the permanent runoff station Antizana 15 (P4 at 4550 m asl). PG began to record data only in April 2002, but these data were found to be in excellent agreement with those collected in P3. P2 was eliminated because the site is too windy, and the P4 series is too discontinuous. In this study, P3 is considered representative of the entire ablation zone. Rain gauges measure cumulative precipitation and are designed to capture both snow and rain during a complete year. The gauges used are cylinders of 150-cm height and with a collecting surface of 2000 cm^2. Each rain gauge is surveyed at the beginning of each month, and the presence of a 2-mm-deep oil layer blocks evaporation. Absence of frozen layers in rain gauges makes the data set accurate over the whole period.

[11] On-site meteorological measurements are recorded by an automatic weather station (AWS) installed in the ablation zone of the glacier (Figure 1). These measurements are discussed in more detail in section 3.3.

[12] Besides local climatic data measured on or near the glacier, we extracted monthly climate data from various gridded data sets, including National Oceanic and Atmospheric Administration (NOAA) interpolated outgoing long-wave radiation (OLR) [*Liebmann and Smith*, 1996], NOAA optimum interpolation SST version 2 (V2) [*Reynolds et al.*, 2002], Climate Prediction Center Merged Analysis of Precipitation (CMAP) precipitation [*Xie and Arkin*, 1997], and temperature, geopotential height, omega vertical velocity, relative and specific humidity, and zonal and meridional wind on all mandatory pressure levels from the National Centers for Environmental Prediction–National Center for Atmospheric Research (NCEP-NCAR) reanalysis [*Kalnay et al.*, 1996]. These data are used to assess the large-scale climate dynamics associated with mass balance variations on Antizana (see section 7).

3.3. Energy Balance Measurements

[13] The energy balance was measured on the glacier surface during a complete annual cycle. A detailed description of the measurement method is given by *Favier et al.* [2004]. Here we only provide a summarized presentation of the different terms of the energy balance. The fluxes toward the surface being positive, the energy balance equation for a melting surface can be written as [e.g., *Oke*, 1987]

$$R + LE + H + P + G = \Delta Q_M, \tag{1}$$

where R is the net all-wave radiation, H the turbulent sensible heat flux, and LE is the turbulent latent heat flux. The heat supplied by precipitation P, even liquid, can be disregarded compared to the other terms of the equation, because the intensity of rain is low, and the temperature difference between rain and glacier surface is small [e.g., *Sicart*, 2002]. The conductive heat flux in the snow/ice G is zero for an isothermal glacier. ΔQ_M is the latent heat storage change due to melting and freezing. The net radiation R is the balance of the incident $S\downarrow$ and reflected $S\uparrow$ short-wave radiation and the incoming $L\downarrow$ and outgoing $L\uparrow$ long-wave radiation:

$$R = S\downarrow - S\uparrow + L\downarrow - L\uparrow = S\downarrow(1-\alpha) + L\downarrow - L\uparrow, \tag{2}$$

where α is the short-wave albedo at the snow/ice surface. The local melting ΔQ_M is derived from measurements recorded by an AWS installed at 4890 m asl in the lower half of the ablation zone of the glacier 15α (Figure 1). Temperature, humidity, wind speed, and the radiative fluxes are recorded by the AWS as half-hourly means integrated

over 15-s time steps. To understand the relation between meteorological conditions and melting, a continuous and complete data set between 14 March 2002 and 14 March 2003 was analyzed extensively by *Favier et al.* [2004]. In addition, other variables including albedo and incoming short-wave and net all-wave radiation were measured between September 1998 and March 2003 to complete the interpretation of the surface energy balance record between March 2002 and March 2003. During the period from March 2002 to March 2003 the four radiative fluxes were directly measured by the AWS, whereas the turbulent heat fluxes were calculated with the bulk aerodynamic approach. The roughness length was calibrated by making direct sublimation measurements on the field with lysimeters during representative periods of the year. In this approach a constant gradient was assumed between the level of the measurements and the glacier surface, and the turbulent heat fluxes were then derived from only one level of measurements.

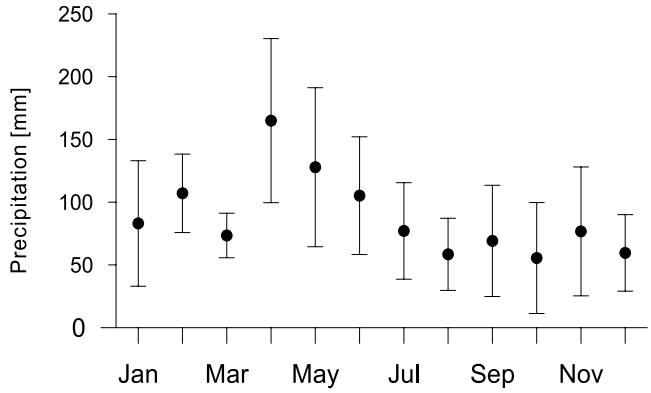

Figure 3. Monthly mean precipitation recorded at the glacier snout (rain gauge P3) averaged over the 1995–2002 period. One standard deviation is indicated (vertical bars).

4. Mass Balance During the 1995–2002 Period

4.1. Seasonal Evolution

[14] Figure 2 displays the mean and the standard deviation of the annual cycle of mass balance measured in the ablation zone. Despite the small amplitude of the mean seasonal cycle (<200 mm w.e. difference between months with highest and lowest mean net balance) a seasonal signal can be identified and the year accordingly divided into four main periods: (1) February, March, April, and May (FMAM) are months with a very high interannual variability, since mass balance oscillates between the equilibrium state and very negative values; (2) JJA are months of moderate ablation and low interannual variability; they represent the core of the "verano" (boreal summer); (3) October and November (ON) is a period of important ablation, but in contrast to FMAM, ablation does not vary a lot from one year to the next; and (4) a significant decrease of ablation rates can be detected in December and January (DJ), during the so-called "veranillo" ("little summer"). September is a highly variable month, which in some years behaves like an extension of the "verano," whereas in other years it may anticipate the negative mass balance of the coming months October–November. This very complex seasonal cycle is in strong contrasts to that observed on outer tropical glaciers, where the seasonality is clearly defined by a high-ablation wet and a low-ablation dry season [*Francou et al.*, 2003].

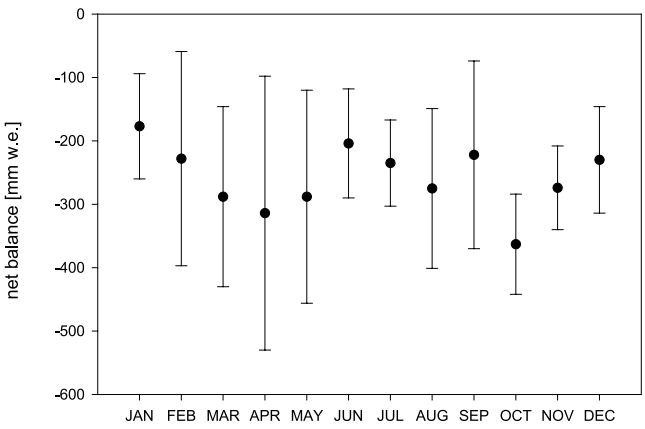

Figure 2. Monthly mean net balance on the ablation zone of Antizana 15α glacier from January 1995 to December 2002 period. One standard deviation is indicated (vertical bars).

[15] Since the most negative mass balances observed in MAM and September–October closely lead or lag the equinoxes, and since only moderate losses are measured in June–July (JJ) and DJ, it is suggested, as a first approximation, that mass balance could be controlled year-round by the top of the atmosphere solar irradiance S_{TOA}. This hypothesis will be discussed further in the context of the energy balance, because the large mass balance variability observed during FMAM and September, with some years even showing positive values, could possibly be explained by the seasonal distribution of precipitation. In Figure 3 the precipitation regime observed at the Antizana site shows a clear maximum in the first rainy season with amounts exceeding 100 mm month^{-1} (except March). The regime with only one pronounced peak of precipitation in the year (March–June) is typical of stations situated on the Amazonian slope of the Andes of Ecuador [*Villacis*, 2001]. However, the April–May peak is marked by a strong interannual variability, which can affect the glacier surface both through changes in cloudiness and snowfall frequency (see section 5). On the other hand, the negative and homogeneous mass balance recorded during the last months of the year, except September, seems to be associated with low precipitation amounts recurring every year. April–May and September encompass the strongest mass balance variability, and it therefore comes as no surprise that the mass balance during these 3 months shows the highest correlation with the annual mass balance as well. As shown in Figure 4, these 3 months alone can explain up to 98% of the variance of the annual mass balance of the ablation zone. However, this does not imply that the other months are of no significance but rather indicates that interannual variability is very similar for each month and that the 12 monthly time series are highly correlated with each other. In fact, the individual monthly time series in February, April–June, and September are all correlated with the annual mass balance at $r > 0.8$. In this context it is further noteworthy that mass loss during 1997 and 1998 was

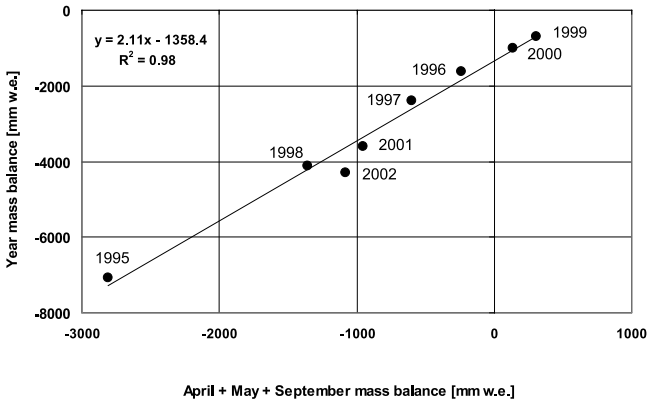

Figure 4. April–May, and September mass balance versus annual mass balance on the ablation zone of Antizana 15α glacier for the 1995–2002 period.

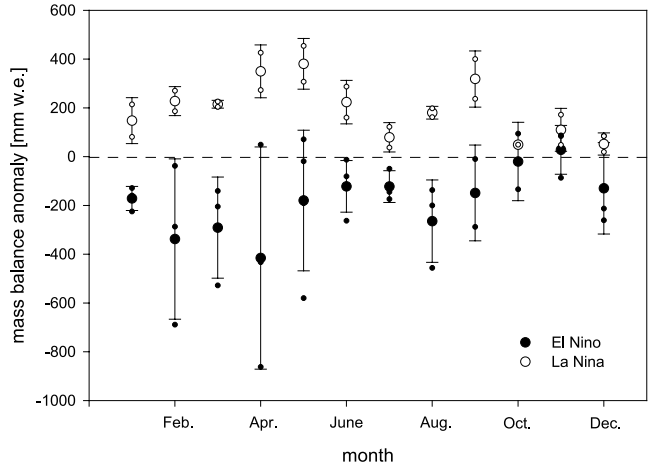

Figure 6. Antizana mass balance anomalies (mm w.e.) in the ablation zone stratified by ENSO events. Individual monthly measurements (small circles), the mean (large circles), and ±1 standard deviation are indicated (vertical bars). El Niño (solid circles) and La Niña events (open circles) are as in Table 1 but shifted by 3 months because of the apparent 3-month lag between tropical Pacific SSTA and mass balance anomalies on Antizana (see text).

by no means extreme but close to average. This suggests that our mass balance record is not significantly biased by the strong and unusual El Niño event of 1997/1998. In conclusion, mean ablation seems to remain at a quite constant level all year round at low elevation, but year-to-year variability shows a distinct seasonal cycle with much larger interannual variations during the key periods FMAM and September.

4.2. Interannual Variations

[16] Monthly mass balance has been highly variable over the period investigated (Figure 5). Strong negative phases occurred in 1995, from mid-1997 to mid-1998, and more recently in 2001 and in 2002. These important losses of mass have been interrupted by periods of balanced or positive mass balance, the most pronounced one lasting from mid-1998 until mid-2000. A 15-month period, beginning at the end of 1995, can be considered as a quasi-balanced period as well. Interestingly, these prolonged periods of negative and positive mass balance coincide with major El Niño (1995, 1997/1998, 2001/2002) and La Niña (1998/2000) events. To illustrate this behavior, we plotted the seasonal mass balance anomalies stratified for El Niño and La Niña periods (Figure 6). These periods are defined according to *Trenberth* [1997] but based on the Niño-4 index (periods when the 5-month running mean of SSTA averaged over the domain 5°N to 5°S/160°E to 150°W remains below (above) −0.4°C (0.4°C) for at least 6 consecutive months) (Table 1). We use the Niño-4 index because regression analyses show highest correlations of the Antizana mass balance record with SSTA in Niño-4 domain (see section 7). In addition, we have also applied a 3-month lag between ENSO phases as defined by SSTA in the Niño-4 domain and our ENSO mass balance composites in Figure 6, as correlation analyses indicate that mass balance anomalies lag tropical Pacific SST by 3 months (see section 7).

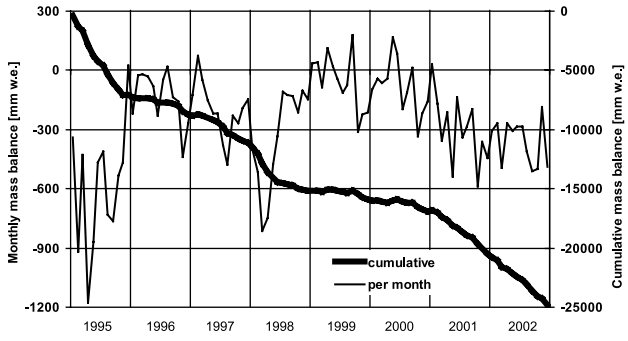

Figure 5. Monthly (thin line) and cumulative (thick line) mass balance of Antizana 15α glacier during 96 months in the ablation zone (January 1995 to December 2002).

[17] While mass balance is negative almost all year round during El Niño periods, it appears to be close to the equilibrium (positive anomalies) during the La Niña periods. Even more striking, however, are the differences that occur in the seasonal cycle during the two opposite phases of ENSO. During El Niño events, February, March, and April (FMA) and August and September (AS) are clearly the months which record the most negative mass balance anomalies, whereas JJ and ON reveal mass balance anomalies closer to zero. La Niña periods, on the other hand, display the almost perfectly opposite pattern, with April–May and September featuring strong positive anomalies and JJA and October, November, and December (OND) being more neutral. This "mirror-shaped" pattern is particularly clear in February–May and in August–September.

[18] Before focusing our analysis on the physical processes at the glacier surface (section 5) and the climatic factors and large-scale circulation which control these processes (sections 6 and 7), we can already draw the following conclusions: (1) ENSO variability strongly impacts the glacier in the ablation zone, with a clear acceleration of ablation processes during warm events, and a more moderate mass loss during cold events; (2) ENSO also affects the mass balance seasonality with enhanced ablation rates in FMAM and AS during warm events, whereas the main ablation tends

Table 1. Neutral, El Niño, and La Niña Periods Between 1995 and 2002[a]

	Neutral	El Niño	La Niña
Time period	June 1995 to Jan. 1997 April 1998 to July 1998 July 2000 to July 2001	Jan. 1995 to May 1995 Feb. 1997 to March 1998 Aug. 2001 to Dec. 2002	Aug. 1998 to June 2000
Total number of months	37	36	23

[a]Periods are according to definition by *Trenberth* [1997] but based on Niño-4 index (SSTA averaged over domain 5°N to 5°S, 160°E to 150°W). Base period for calculation of anomalies is 1950–1979.

to be shifted toward the solstice months during the cold events; (3) mass balance variability increases during ENSO periods, particularly during the first semester in February–May; and (4) neutral ENSO situations, which represent more than a third of the data set (Table 1), do not seem to exhibit strong anomalies (not shown).

5. Energy Fluxes and Ablation Cycle at the Glacier Surface

[19] To understand the mass balance variability presented in the previous section, we need to analyze the ablation processes taking place at the glacier surface. This analysis is based on the well-documented cycle March 2002 to March 2003, during which the main terms of the energy balance were measured. Details of this analysis can be found in a companion paper by *Favier et al.* [2004]. To extend these observations back in time to 1995, we relied on data from the NCEP-NCAR reanalysis and outgoing longwave radiation (OLR) measured by satellites. Prior to using these proxies, we evaluate in section 5.1 how well they correspond with our own field measurements in 2002/2003.

5.1. Main Variables of the Ablation Process

[20] During the 2002–2003 cycle the net short-wave radiation (S) was the main influx to the surface (123 W m^{-2}). This contribution was partly compensated by the long-wave radiation (L) heat sink (-39 W m^{-2}). The total net all-wave radiation ($R = 84$ W m^{-2}) largely dominated the ablation processes with only a minor contribution from the turbulent heat fluxes ($LE + H = -6$ W m^{-2}), except during June, July, August, and September (JJAS) when winds are strong [*Favier et al.*, 2004].

5.1.1. Turbulent Heat Fluxes

[21] Turbulent heat fluxes are negligible during periods with low winds. During windy periods, sensible and latent turbulent heat fluxes increase in similar proportion, but H does not compensate LE completely, hence $LE + H$ always represents a heat sink. Thus we view the latent turbulent heat fluxes LE as representative of the total turbulent heat fluxes. The latent turbulent heat fluxes depend basically on wind velocity and humidity. During the 2002–2003 cycle these fluxes could not be disregarded, particularly during the windy periods. In fact, when easterlies are strong, as in 2002 between 1 June and 15 October, sublimation becomes a significant term in the energy balance and leads to ablation rates as high as 3 mm w.e. d^{-1}. An important sink of energy is hence associated with this process, estimated as $LE \approx -100$ W m^{-2}, which contributes to reduce melting during the "verano" months. In order to quantify the turbulent fluxes during 1995–2002 we extracted the reanalyzed wind speed and specific humidity data at the 500-hPa level from the grid cell closest to Antizana (77.5°W, 0°S) and calculated the following sublimation index β:

$$\beta = (q - q_s)v, \tag{3}$$

where q is the monthly mean specific humidity, q_s is the surface specific humidity of a snow/ice surface in melting conditions at 500 hPa, and v is the wind speed. The more negative the index, the more sublimation occurs. We are aware of the fact that this empirical index does not physically describe the sublimation process at the glacier surface. However, over the 2002–2003 period, correlation between the β index and the turbulent fluxes at the glacier surface is high, with $r = 0.78$ ($p = 0.01$) (Figure 7a). The

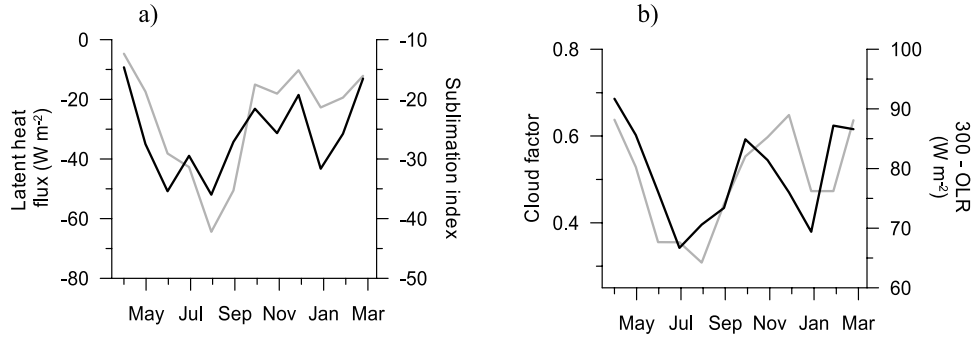

Figure 7. Comparison between monthly mean field measurements and proxy values derived from National Centers for Environmental Prediction–National Center for Atmospheric Research (NCEP-NCAR) reanalysis between April 2002 and March 2003. (a) Comparison between the measured turbulent latent heat flux (gray line) and the sublimation index β (black line). (b) Cloud factor (gray line), deduced from field measurements, and outgoing longwave radiation (OLR) values reduced from 300 W m^{-2} (black line). See text for details.

turbulent heat fluxes observed during the 2002–2003 cycle occur every year on the same order of magnitude. The maximum values always occur between June and September, but the start and end date of increased sublimation can vary considerably. The lowest sublimation is always recorded in October and November. As a consequence, JJAS is the only period during which sublimation can lead to a significant reduction of melting.

5.1.2. Net Radiation: Incoming Fluxes and Cloudiness

[22] With a mean slope of 18° and a NW orientation the strength of the incoming short-wave radiation increases on the glacier 15 from April to August. On the other hand, a slight minimum occurs during the "veranillo" December–January. The energy influx, however, is modulated by cloud cover, which, on Antizana glaciers, is a good proxy for the amount of incoming radiation. Both incoming long-wave $L\downarrow$ and short-wave $S\downarrow$ fluxes are related to cloud cover, $S\downarrow$ negatively, $L\downarrow$ positively. However, changes in $S\downarrow$ are much larger and therefore control the incoming flux rates. By comparing $S\downarrow$ with S_{TOA}, a "cloud factor" cf can be obtained, defined as $cf = 1.3 - 1.4S\downarrow/S_{TOA}$, which represents a quantitative cloud cover estimate. The values 1.3 (offset) and 1.4 (scale factor) were derived from a simple linear optimization process [see *Favier et al.*, 2004]. Cloud cover during the 2002–2003 cycle shows two maxima, one around March and another one around November (Figure 7b), when the S_{TOA} is close to its maximum. Conversely, a clear minimum was observed in June, July, and August. This is consistent with the seasonal distribution of precipitation during the studied cycle (not shown). Correlation of OLR, which is a good proxy for convective activity and precipitation [e.g., *Liebmann et al.*, 1998], extracted from the grid cell centered over the Antizana region with the cloud factor shows a good agreement ($r = -0.68$, $p = 0.05$) between the two data sets in 2002/2003 (Figure 7b). Clearly, low OLR values coincide with high cloud cover and vice versa. Consequently, OLR is also significantly correlated with $S\downarrow$ ($r = 0.60$, $p = 0.05$) and $L\downarrow$ ($r = -0.84$, $p = 0.001$). The seasonal cycle of OLR is very similar to the one in 2002/2003 in each of the 8 years, 1995–2002 (not shown). Largest interannual cloud cover variability occurs around March and September (equinox), whereas the higher OLR values between May and August show less variance. Hence incoming fluxes are highest during the "verano," are highly variable during the equinox, and feature a slight minimum in December–January.

5.1.3. Net Radiation: Net All-Wave Radiation and Albedo

[23] As shown by *Favier et al.* [2004], the seasonal evolution of albedo controls the net short-wave radiation ($r = -0.80$, $n = 359$; daily values, $p = 0.001$) and hence melting rates on the glacier. Albedo is extremely variable and depends on the occurrence of snowfall. After snowfall, the albedo reaches values up to 0.9, and melting stops. After long periods without snowfall the albedo of the snow first progressively degrades to values close to 0.5–0.6 and then abruptly decreases to 0.3 when the bare ice is exposed at the glacier surface. Melting rates closely follow the change in albedo; hence snowfall frequency plays a key role in the surface energy balance. In order to verify the role of albedo in melting, the analysis of short-wave radiation was extended back to September 1998. Months with data lacking for more than 10 days were removed; thus 37 months of data obtained from the AWS were analyzed. This analysis confirms that the mean net all-wave radiation and mass balance are highly correlated on intraseasonal (monthly) timescales ($r = -0.90$, $p = 0.001$). This highly significant relationship is by and large due to the important link that exists between albedo and mass balance ($r = 0.87$, $p = 0.001$).

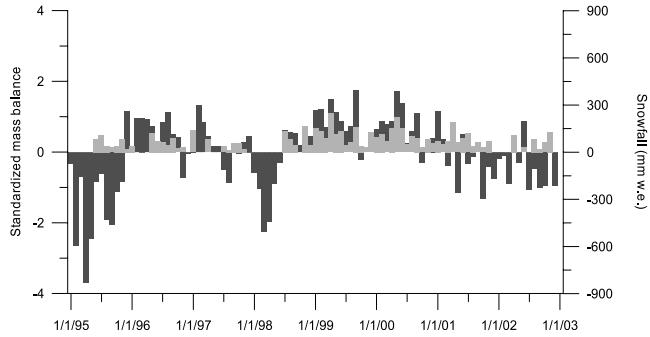

Figure 8. Monthly mass balance anomaly (black) and snowfall amount (gray). Snowfall is separated from rain by a using temperature threshold of 0.5°C. Reanalyzed temperature is increased by 5.3°C to fit the observed temperature at the glacier surface. See text for details.

5.1.4. Temperature Dependence of Snowfall/Rainfall Occurrence

[24] No real dry season exists on Antizana, since at least 50 mm w.e. of precipitation falls in each month. However, precipitation on the glacier is not always solid. Vertical oscillations of the 0°C isotherm displace the snow/rain limit up and down the glacier. Temperature controls the phase of precipitation and hence the melting rates via the albedo [*Favier et al.*, 2004]. In order to verify this field observation over a longer period of time we used the NCEP-NCAR data set to correlate monthly reanalyzed temperature at the 500-hPa level in the grid cell closest to Antizana and monthly temperature data from the AWS since September 1998. Although thermal conditions in the free atmosphere and in near-surface levels are different, the reanalyzed temperature correctly reproduces both seasonal and interannual temperature variations observed in the surface boundary layer ($r = 0.71$, $p = 0.01$). However, the two temperature series are offset, with the monthly mean temperature at the AWS being 5.3°C higher than the temperature of the free atmosphere at the 500-hPa level. Hence we reconstruct a set of "corrected temperature" on the Antizana site for the considered period by adding 5.3°C to the reanalysis data. These corrected temperature data can be used to determine the temperature threshold at which precipitation changes from liquid to solid and vice versa, as mass balance, albedo, and snowfall should be highly correlated at times when all precipitation falls in the form of snow. On the basis of a tuned optimization process, *Favier et al.* [2004] determined that a temperature threshold of 0.5°C yields the highest correlation between daily values of snowfall and albedo. Here we use the same threshold to compare monthly mass balance and snowfall occurrence (Figure 8). When the "corrected temperature" exceeds 0.5°C, rain is dominant, and mass balance, via the albedo, becomes negative, whereas at lower

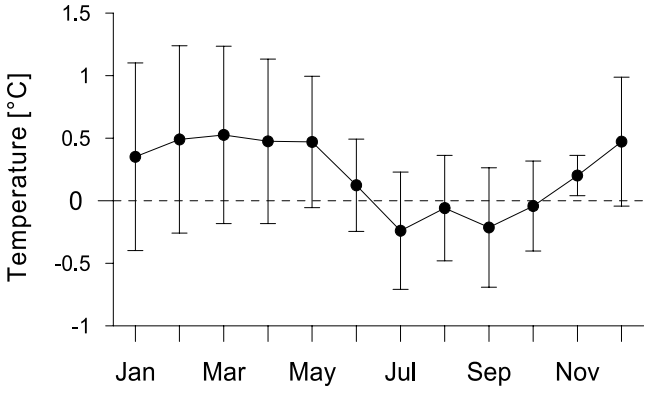

Figure 9. Monthly mean reconstructed temperature (°C) in grid cell nearest Antizana (77.5°W, 0°S) averaged between 1995 and 2002. One standard deviation is indicated (vertical bars). A constant value of 5.3°C has been added to the 500-hPa reanalysis data to account for the offset between NCEP-NCAR and automatic weather station (AWS) data (see text for details).

temperature, snowfall leads to an abrupt decrease of melting. Since temperature controls the phase of precipitation, albedo and precipitation are better correlated if we only consider the months with temperature below 0.5°C (r = 0.51, p = 0.01). Precipitation and mass balance are also well correlated during these "cold months" (r = 0.52, p = 0.01). Nevertheless, in some cases such as during the second part of 1995, this distinction between snow and rain cannot explain the strong negative mass balance observed in Figure 8. In this case, a deficit of precipitation offers a better explanation of the strong mass loss.

[25] In conclusion, the following factors tend to accelerate melting at the glacier surface: (1) air temperature above 0.5°C near the ablation area, as it favors rain over snowfall, (2) weak and sporadic snowfalls, insufficient to maintain a high glacier albedo, (3) low wind speeds, which limit the transfer of energy from melting to sublimation, and (4) low cloud cover, which increases the incoming short-wave radiation, a factor particularly efficient during the periods close to the equinoxes.

5.2. Typical Ablation Cycle

[26] Compared to the outer tropical areas Bolivia and Peru, the seasonality of climate is weak in Ecuador [*Wagnon et al.*, 1999; *Francou et al.*, 2003]. However, the thermal variability associated with the change of phase of precipitation induces a marked seasonality of the melting processes at the glacier surface. In order to summarize this seasonal ablation cycle and its variability over time we next briefly discuss its principal characteristics during key times of the year. Three principal periods have been distinguished, which are closely tied to the mass balance evolution defined in the section 4.1.

5.2.1. Key Months April–May and September (AMS)

[27] As shown in Figure 4, mass balance variability in AMS is most closely related to the annual mass balance variance. April and May are characterized by strong interannual precipitation and temperature variability (Figures 3 and 9). If air temperature is low (well below 0.5°C) and if precipitation is frequent, a long-lasting snow cover develops on the glacier, and albedo remains permanently high. In this case, melting is very reduced. On the other hand, if temperature is well above the threshold of 0.5°C, precipitation will be mostly liquid and hence albedo is lowered as bare ice becomes more and more exposed up to 5000 m. If, at the same time, a deficit of precipitation and low cloud cover prevails, melting is greatly enhanced because of the higher solar irradiance during the equinoctial period. In September and, to a lesser extent, in August, temperature variability is lower (Figure 9), and albedo variations are primarily controlled by the frequency and intensity of snowfall. However, higher sublimation rates in September contribute to reduced overall ablation compared to April–May.

5.2.2. Summer Months JJA

[28] During the slight thermal minimum of July–August the year-to-year variability of temperature is reduced (Figure 9). At this time of year, precipitation preferentially falls as snow, thereby increasing the albedo. Although cloud cover is generally low and hence incoming short-wave radiation is strong, the high albedo values limit the net all-wave radiative budget. In addition, wind speed tends to peak in JJA, which leads to enhanced sublimation, thereby further reducing melt rates. This explains why JJA is normally a period of low ablation. Nevertheless, snowfall in JJA is scarce and does not preclude a slow degradation of the albedo at the glacier surface, which in turn leads to a gradual increase in melt rates toward August.

5.2.3. October–March Period

[29] Even though precipitation can be significant in October and November, mass balance is always very negative in this period; however, more moderate conditions progressively appear in December and January. This secondary precipitation maximum in November, unlike the one between February and June, is limited in time and in quantity. Although temperature is low (Figure 9) and allows that most of the precipitation falls in the form of snow, melting can still increase significantly if sublimation is low. If precipitation falls in September, sublimation rates may still be high enough to reduce melting substantially, but if precipitation falls in October or in November when sublimation is already very low (Figure 7a), the fresh snow blanket will rapidly disappear and thereby lead to high ablation rates. December and January (the "veranillo" period) repeat the situation of the "verano" but with low winds (not shown) and low sublimation (Figure 7a) [*Favier et al.*, 2004]. Following January, the mass balance variability increases and begins to reflect the typical instability of temperature and precipitation of the first semester.

[30] In conclusion, wind speed (not shown) and cloud cover are the main climatic variables that show a pronounced seasonality in the highlands of Ecuador. We can distinguish a well-defined windy period from June to September with strong sublimation and the rest of the year which features only limited turbulent heat fluxes. Linked to wind strength, cloudiness also shows important seasonal variations. Other factors such as temperature, precipitation, and humidity have more subtle variations. Nevertheless, the interannual variations of these parameters are strong and, when interacting with each other, they can develop important feedbacks. As shown in section 5.1.4, this is the case, for instance, between temperature and precipitation when a certain temperature threshold is reached. Hence it is no

surprise that ablation varies the most around the time of the equinoxes, in particular during April–May and September. These are the months that show important interannual variations in temperature, precipitation, and cloudiness and at the same time feature the highest S_{TOA}.

6. Typical Responses of the Glacier Mass Balance to Extreme ENSO Situations

[31] Once the ablation processes and their interannual variability have been identified, it is possible to specify how the extreme phases of ENSO can impact the glacier evolution. Let us recall that the separation between El Niño and La Niña periods is based on the criteria by *Trenberth* [1997] for the Niño-4 sector and that the SSTAs lead Antizana mass balance by 3 months (see section 4.2).

6.1. Glacier Mass Balance During La Niña Periods

[32] Monthly mass balance and precipitation are highly correlated ($r = 0.76$, $p = 0.001$) during La Niña periods as defined in Table 1. On the other hand, no significant correlation exists between the two variables during El Niño. The positive correlation during La Niña is due to the negative temperature anomalies between January and May and in September (Figure 10a), causing all precipitation to fall in the form of snow. Furthermore precipitation amounts are above average during La Niña periods (Figure 10b); hence the snow tends to form a continuous and permanent blanket with high albedo on the glacier surface, typically in April, May, June, and August–September. The increased cloud cover and accordingly the reduced short-wave incoming radiation also play a role for reducing melt rates in January–February and September (Figure 10c). On the other hand, strong winds begin earlier and end later than average and typically last from March to October (Figure 10d). Compared with El Niño periods, the stronger sublimation anomaly occurs in March and August (Figure 10e). During the core of the windy period ("verano") the low specific humidity combines with the wind to strengthen sublimation (not shown). In July, August, and OND, temperature and precipitation do not exhibit marked differences between the two phases of ENSO, and hence the mass balance is quite similar during both periods.

[33] In conclusion, La Niña events are characterized by cold temperatures, abundant snowfall, and, to a lesser degree, more constant winds (see section 7). These factors combine to increase albedo and sublimation and therefore preclude melting at the glacier surface. Under such conditions the snow line drops to the lower reaches of the glacier, and snow will cover the glacier terminus during several weeks. Mass balance variations in these circumstances first and foremost reflect the excess of precipitation, particularly from January to June and in August–September. In 1999, for example, the mass loss at the lowest stakes was only 2000 mm w.e., which is 3 times less than during a typical El Niño year, and the ELA dropped to 4960–4980 m, only 150 m above the glacier terminus.

6.2. Glacier Mass Balance During El Niño Periods

[34] From January to May and in September, air temperature is 1°–2°C higher during El Niño as compared to La Niña periods (Figure 10a). As a consequence the snow-rain limit rises up to 5000–5100 m asl, lowering the albedo and enhancing the absorption of energy by the glacier surface. The fact that precipitation decreases almost every month during El Niño periods, particularly during the key months April and September (and also in January), has

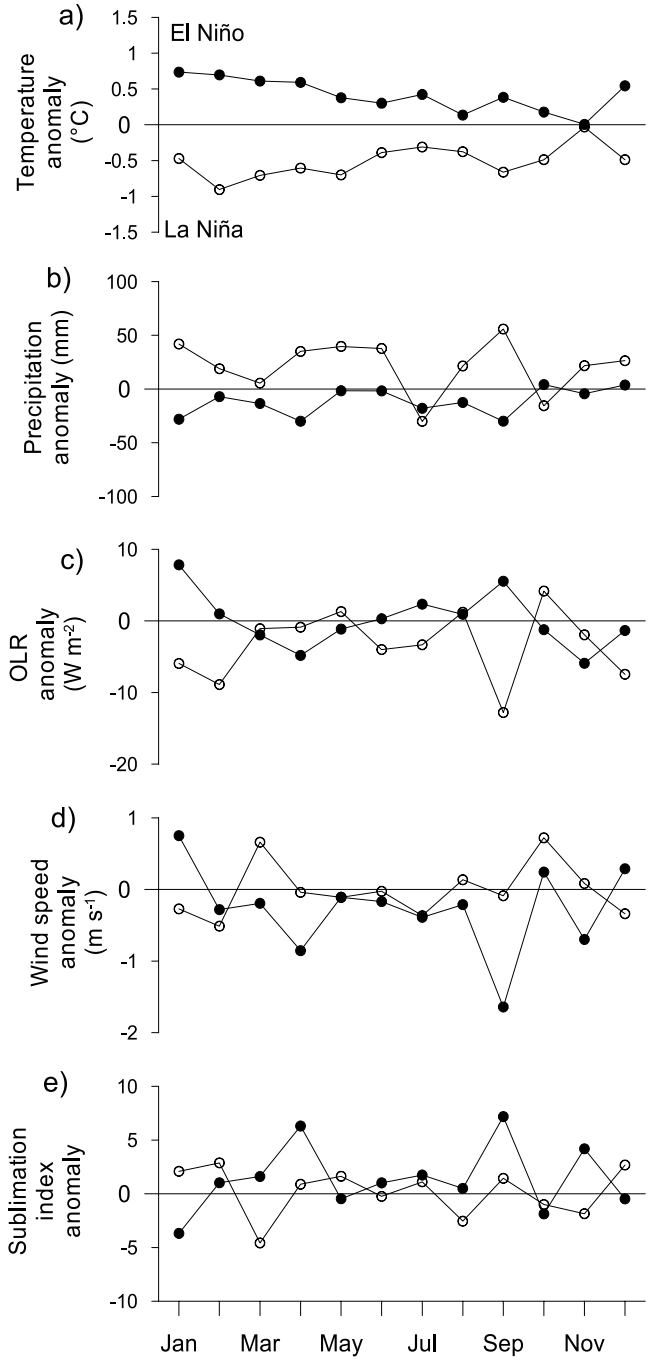

Figure 10. Monthly mean anomalies during La Niña (open circles) and El Niño (solid circles) for (a) NCEP-NCAR 500-hPa temperature (°C), (b) precipitation (mm) at 4650 m asl, (c) OLR (W m^{-2}), (d) NCEP-NCAR 500-hPa wind speed (m s^{-1}), and (e) sublimation. (Note that sublimation increases when values are more negative.) Reanalysis and OLR data are from grid cell closest to location of Antizana. See text for details.

important implications for the mass balance (Figure 10b). Large positive OLR departures in January and September confirm that cloud cover is indeed reduced and that shortwave radiation receipts are higher during El Niño (Figure 10c). High winds are limited to the core of the "verano" (JJA) and May, unlike La Niña periods where winds are also high during April and September (Figure 10d). The lower wind speed in April and September induces a sublimation decrease, which in turn tends to enhance ablation rates as the entire available energy is consumed by the much more energy-efficient melting (Figure 10e). As shown by the sublimation index, however, the energy sink due to the turbulent fluxes limits melting and thereby contributes to the mass balance equilibrium between June and August. The low variability of mass balance in JJA is thus maintained by the weak temperature and precipitation anomalies. The same climatic control operates in OND, when precipitation and temperature variations are also minor, regardless of the phase of ENSO (Figures 10a and 10b).

[35] In conclusion, El Niño periods are characterized by increased melt rates. This situation is caused both by rainfall on the glacier due to higher temperatures as well as by a deficit of precipitation, both of which contribute to lowering the albedo over large areas of the glacier. A significant reduction in cloud cover during the equinoxes has an important effect on the amount of incoming shortwave radiation. Hence mass balance tends to follow the seasonal cycle of the S_{TOA}, and melting is highest around the equinoxes AMS and minimal around the solstices July–August and DJ. Although sublimation still represents a heat sink, the turbulent heat fluxes limit sublimation to a shorter period (JJA), and melting is more efficient than during La Niña. As a consequence the glacier experiences an important mass loss in its lowest parts, with rates that exceeded 6000 mm w.e. near the snout in 1995, 1997, and 1998. At the same time the ELA rises up above 5100 m asl (when in equilibrium, the ELA is located at 5030 m asl), and the ablation zone can extend to more than 40% of the total area (when in equilibrium, the ablation zone only represents 27% of the total area).

7. Glacier and Large-Scale Climate

[36] Since ENSO appears to be having such a profound impact on the mass balance of Antizana glacier, the large-scale atmospheric circulation must be altered in a significant way aloft the Andes of Ecuador during the extreme phases of ENSO. At the same time it is also possible that forcing mechanisms other than ENSO may contribute significantly to intraseasonal and interannual climate variability in the Ecuadorian Andes [*Vuille et al.*, 2000b] and hence impact mass balance on Antizana. To shed some light on these questions, we first investigate the relationship between interannual mass balance variations and tropical SSTA and then establish a link between SSTA and glacier mass balance through a regression analysis of the associated atmospheric circulation dynamics. Since we are primarily interested in the interannual variations in this section, the following analyses are all based on monthly anomalies, with the seasonal cycle removed.

[37] Correlation of the mass balance record with tropical SSTA shows that highest correlations occur in the Niño-4

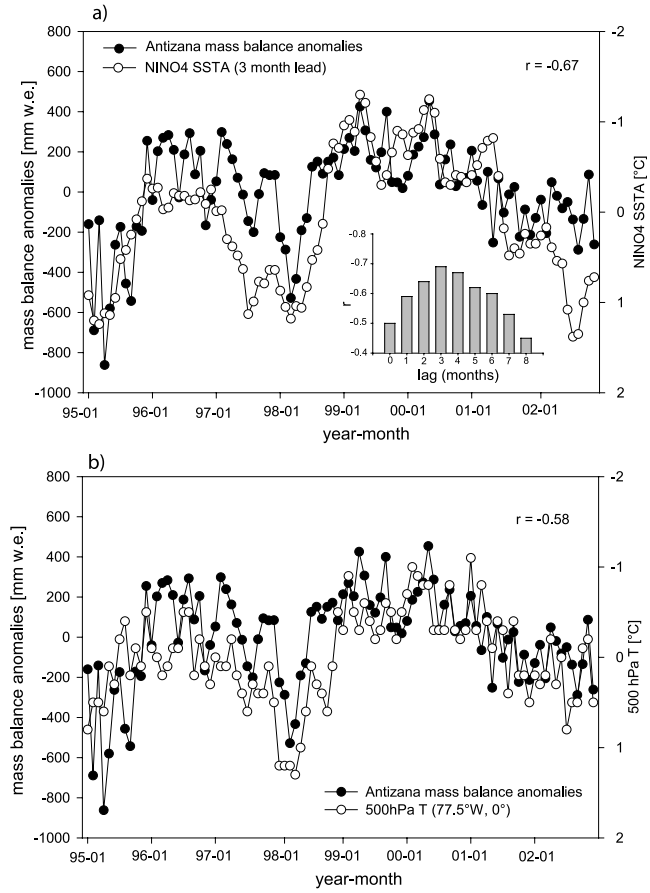

Figure 11. (a) Time series of monthly mass balance anomalies (mm w.e., solid circles) on Antizana glacier and Niño-4 SSTA (°C, open circles) between January 1995 and December 2002. Mass balance anomalies lag SSTA by 3 months. Scale for SSTA (right side *y* axis) is reversed. Vertical bar plot (inset) shows correlation between mass balance anomalies and Niño-4 index, with Niño-4 index leading mass balance anomalies between 0 and 8 months. (b) As above, except for comparison between Antizana mass balance anomalies and monthly NCEP-NCAR reanalysis 500-hPa temperature (°C, open circles) in grid cell nearest Antizana (77.5°W, 0°S). Scale for temperature anomalies (right side *y* axis) is reversed.

domain (5°N to 5°S, 160°E to 150°W) in the central equatorial Pacific. Lead-lag correlation analyses further indicate that SSTAs in the Niño-4 domain lead mass balance anomalies by 3 months (Figure 11a). This apparent lag suggests that air temperature may be involved in order to explain the SSTA–mass balance relationship, as temperature anomalies in the tropical troposphere are known to lag equatorial Pacific SSTs by 1–3 months [e.g., *Kumar and Hoerling*, 2003]. Indeed, 500-hPa temperature aloft the Ecuadorian Andes also lags the Niño-4 index by 3 months (not shown). On the other hand, mass balance anomalies are also closely correlated with nearby 500-hPa temperature, with no apparent delay (Figure 11b). A simple linear correlation analysis indicates that 45% of the variance observed in the mass balance record can be explained by SSTA in the Niño-4 domain ($r = -0.67$, $p = 0.01$). While

ENSO affects the local climate near Antizana in various different ways (see below), temperature anomalies seem to have the most profound effect on mass balance variability, explaining 34% of the variance in annual mass balance ($r = -0.58$, $p = 0.01$). This result is consistent with the temperature effect on the rain-snow line discussed earlier in sections 5 and 6. The 3-month lag between tropical Pacific SSTA and mass balance variability may also offer some clues to the observed seasonal dependence of both mass balance and mass balance variability. As shown previously in Figure 6, the largest differences in mass balance between the two phases of ENSO occur from February to May. This is consistent with the delayed atmospheric response indicated above, because both La Niña and El Niño are to some extent phase locked to the annual cycle and tend to peak in boreal winter (between November and February). Hence the largest impact on mass balance occurs with a 3-month delay around February–May. Indeed this is the time when temperature anomalies between the two phases are largest in the Andes of Ecuador (Figure 10a). This delayed ENSO impact has further ramifications as the largest temperature departures coincide with the April–May (AM) rainy season (Figure 3), which will further enhance mass balance anomalies due to increased (decreased) precipitation associated with El Niño (La Niña) and the associated changes of the glacier albedo.

[38] If ENSO is indeed by far the most important factor affecting mass balance variability on Antizana 15, then both tropical SST and atmospheric circulation patterns associated with mass balance variations must resemble the known response to canonical ENSO events. This hypothesis can easily be tested by comparing ENSO composites (representing the difference in the mean atmospheric and oceanic conditions between La Niña and El Niño events as defined in Table 1) with the Antizana correlation and regression field (Antizana mass balance anomalies regressed upon these same atmospheric and oceanic variables and indicating the sign, strength, and significance of the local anomaly (e.g., wind anomaly) associated with a 1-m w.e. anomaly in the mass balance time series). These comparisons are shown in Figures 12, 13, and 14.

[39] Correlation of the mass balance anomalies with tropical SSTA (Figure 12a) and accounting for the 3-month lag yields the typical broad ENSO tongue, with negative correlations extending from the west coast of South America westward along the equator beyond the dateline. To the north and south of this wedge-shaped pattern, positive correlations extend from 160°E into the subtropics of both hemispheres. This pattern is consistent with the canonical ENSO structure described in many previous studies [e.g., *Garreaud and Battisti*, 1999; *Enfield and Mestas-Nuñez*, 1999], resembles the ENSO composite over the same time period (Figure 12b), and thus confirms that positive mass balance departures are indeed associated with cold tropical Pacific SSTA and vice-versa.

[40] The change in the Walker circulation associated with ENSO during the 1995–2002 period lead to suppressed convection and increased subsidence over the central equatorial Pacific during La Niña, while at the same time convection and midtropospheric upward motion were enhanced over the Amazon basin and extended into the southern Caribbean, the subtropical Andes, and the equatorial Atlantic (Figure 12d), consistent with earlier studies [e.g., *Kousky and Kayano*, 1994]. If mass balance anomalies from Antizana 15 are regressed upon these variables, an almost identical picture emerges (Figure 12c), confirming the dominant impact of ENSO. This pattern suggests that the enhanced precipitation observed on Antizana during La Niña periods (Figure 10b) is due to increased convection over the entire Amazon basin and extending westward over the tropical and subtropical Andes. Repeating this analysis with CMAP precipitation instead of OLR data yields similar results (not shown).

[41] The lower tropospheric circulation reflects the shift in the Walker circulation and the steepened E–W pressure gradient associated with the positive phase of the Southern Oscillation during La Niña events (Figure 13d). As a result, SE and NE trades are strengthened in the subtropics of both hemispheres converging in equatorial easterly anomalies downstream. In the upper troposphere the La Niña–related cooling extends throughout the tropical Pacific–South America domain and, combined with the warming in midlatitudes over the Pacific, leads to a weakened meridional temperature gradient and therefore subdued subtropical jets in both hemispheres (Figure 13b). The cyclonic rotation about two distinctive negative anomalies centered near 140°W and 15°S and 15°N over the central tropical Pacific reflects a typical ENSO-related dynamic response to changes in convection over central tropical Pacific [*Yulaeva and Wallace*, 1994]. The atmospheric circulation aloft the equatorial Andes is characterized by cooler conditions and enhanced upper air easterly winds during La Niña, consistent with the results presented in Figure 10. All these ENSO characteristics of the lower and upper tropospheric circulation are reproduced in the mass balance regression fields (Figures 13a and 13c) rendering further evidence for the notion that ENSO is by and large dictating the interannual variations of Antizana 15 mass balance.

[42] A vertical cross section through the tropical troposphere along the equator and across the Andes from the Pacific (90°W) to the Amazon basin (70°W) completes this picture (Figure 14). Increased upward motion over the Amazon basin and strengthened upper air easterlies aloft the equatorial Andes characterize both the ENSO composite (Figure 14b) and the Antizana mass balance regression field (Figure 14a), although the layer of significant easterly wind anomalies is shallower in the regression field and significant upstream and downstream of the Andes only. Both patterns also feature a strengthening of the midtropospheric northerly wind component near the Andes. The enhanced easterly flow and the increase in convection over the Amazon basin to the east of the Andes, in conjunction with significantly lowered temperatures (0.8°–1.0°C lower during La Niña as compared to El Niño), lead to a significant increase in relative humidity in midtropospheric levels upstream and near the Andes (Figure 14d), a pattern which is clearly reproduced in the mass balance regression field (Figure 14c).

8. Summary and Conclusion

[43] Here we present a new, continuous, monthly mass balance record from the ablation zone of Antizana 15 glacier in the Andes of Ecuador, measured between January 1995 and December 2002. This 96-month period was

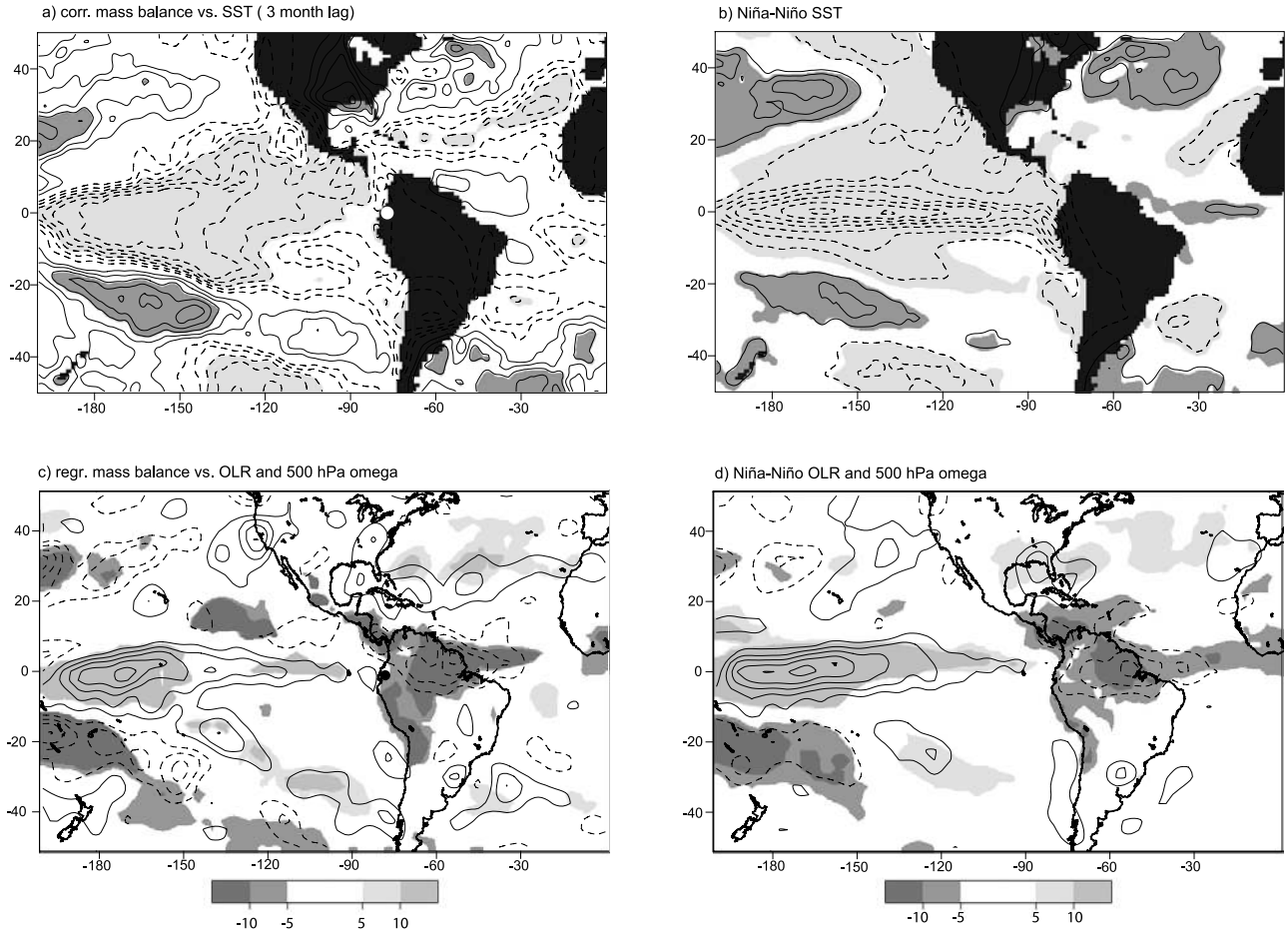

Figure 12. (a) Correlation field between monthly Antizana mass balance anomalies (location indicated by white dot) and monthly National Oceanic and Atmospheric Administration (NOAA) Optimum Interpolation SSTA V2 between January 1995 and December 2002. The 3-month lag between Antizana mass balance anomalies and SSTA is accounted for. Contour interval is 0.1; negative contours are shown (dashed), and zero-contour line is omitted. Correlation coefficients >0.4 (<−0.4) are significant at $p < 0.05$ assuming 3 degrees of freedom per year and shaded in dark (light) gray, respectively. (b) As in Figure 12a but for La Niña–El Niño composite based on ENSO periods as defined in Table 1. Contour interval is 0.4°C; 0°C contour line is omitted, and negative contours are shown (dashed). Regions where SSTs are significantly higher (lower) during La Niña as compared to El Niño based on two-tailed Student's t test (at $p = 0.05$ level) are shaded in dark (light) gray. (c) Antizana mass balance anomalies regressed upon NOAA interpolated OLR and NCEP-NCAR 500-hPa omega vertical velocity anomalies between January 1995 and December 2002. Regression coefficients indicate local anomalies associated with a 1-m w.e. anomaly in the Antizana mass balance (location indicated by black dot). OLR anomalies are only shown if >5 W m^{-2} per m w.e. or <−5 W m^{-2} per m w.e. (see scale below) and local correlation coefficient is significant at $p = 0.05$ level. Vertical velocity anomalies are indicated by contour lines. Contour interval is 0.01 Pa s^{-1} per m w.e.; zero-contour line is omitted, and negative contours are shown (dashed). (d) As in Figure 12b except for NOAA interpolated OLR and NCEP-NCAR 500-hPa omega vertical velocity. OLR values are only shown if >5 W m^{-2} or <−5 W m^{-2} (see scale below) and difference between La Niña and El Niño periods is locally significant at $p = 0.05$ level based on two-tailed Student's t test. Contour lines indicate 500-hPa omega vertical velocity difference (La Niña–El Niño). Contour interval is 0.01 Pa s^{-1}; zero-contour line is omitted, and negative values are shown (dashed).

marked by alternating warm, cold, and neutral ENSO phases. Highest ablation rates were observed during the El Niño events of 1995, 1997/1998 and 2001/2002 but were interrupted by periods of balanced or positive mass balance, the most marked one lasting from mid-1998 until mid-2000, coincident with the 1998–2000 La Niña. During the 8-year period studied, mass balance was negative all year round during El Niño periods but remained close to equilibrium (positive anomalies) during La Niña events.

[44] On seasonal timescales, mean ablation rates remain at a quite constant level all year round, but interannual variability shows a distinct seasonality with much larger changes

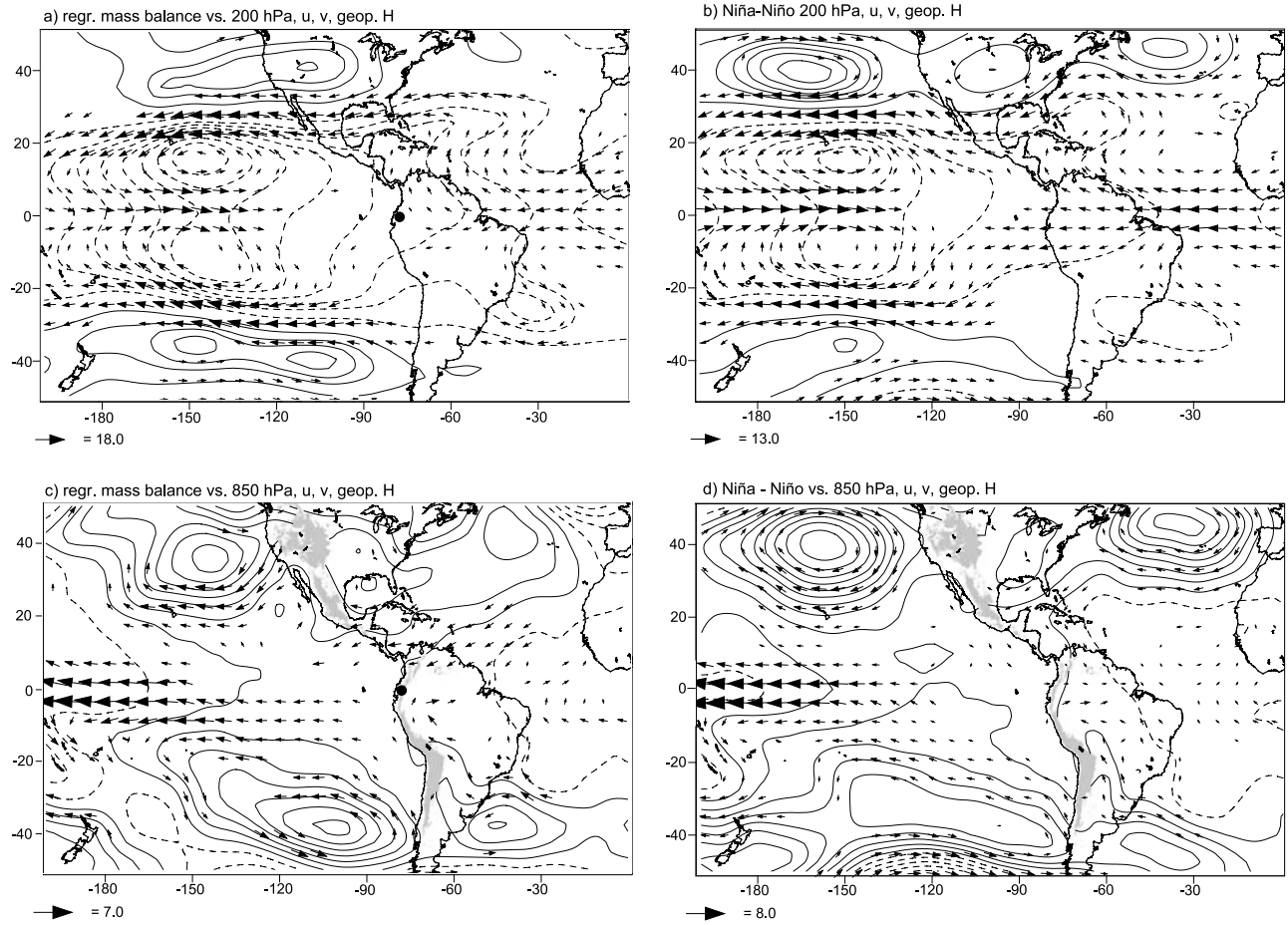

Figure 13. (a) Antizana mass balance anomalies regressed upon NCEP-NCAR 200-hPa geopotential height and wind anomalies between January 1995 and December 2002. Regression coefficients indicate local anomalies associated with a 1-m w.e. anomaly in the Antizana mass balance time series (location indicated by black dot). Wind anomalies are only shown if either zonal or meridional wind component is significantly correlated with Antizana mass balance time series at $p = 0.05$ level. Scale for wind vector (m s^{-1} per m w.e.) is shown below. Geopotential height anomalies are indicated by contour lines. Contour interval is 20 gpm per m w.e. and 10 gpm per m w.e. when >50 gpm (<−50 gpm), respectively. Zero-contour line is omitted, and negative contours are shown (dashed). (b) La Niña–El Niño composite difference in NCEP-NCAR 200-hPa geopotential height and wind (1995–2002), based on ENSO periods as defined in Table 1. Wind vectors are only shown if either zonal or meridional component is significantly different during La Niña as compared to El Niño based on two-tailed Student's t test (at $p = 0.05$ level). Scale for wind vectors is given below. Contour interval for geopotential height is 20 gpm and 10 gpm when >50 gpm (<−50 gpm). Zero-contour line is omitted, and negative contours are shown (dashed). (c) As in Figure 13a except for 850-hPa level and with contours for geopotential height anomalies every 4 gpm per m w.e.; negative contours are shown (dashed). Cordillera > 1500 m is indicated (gray shading). (d) As in Figure 13b except for 850-hPa level and with contours for geopotential height anomalies every 4 gpm; negative contours are shown (dashed). Cordillera > 1500 m is indicated (gray shading).

from year to year during the key periods FMAM and September. This variability is caused by large differences that occur in the seasonal cycle during the two opposite phases of ENSO. During El Niño events the most negative mass balance anomalies are recorded during FMA and AS, whereas during the rest of the year, mass balance anomalies are close to zero. During La Niña periods this ablation pattern is almost completely reversed with large positive mass balance anomalies during April–May and September, while ablation during the other parts of the year is more neutral.

[45] Energy balance studies at the glacier surface indicate that several factors contribute to accelerated melting and hence a more negative mass balance: (1) air temperature above 0.5°C near the ablation area, as it favors rain over snowfall, (2) weak and sporadic snowfall, insufficient to maintain a high glacier albedo, (3) low cloud cover, which increases the incoming short-wave radiation, (4) low wind speeds, which limit the transfer of energy from melting to sublimation. As temperature, precipitation and cloud cover all show largest interannual variations around the time of

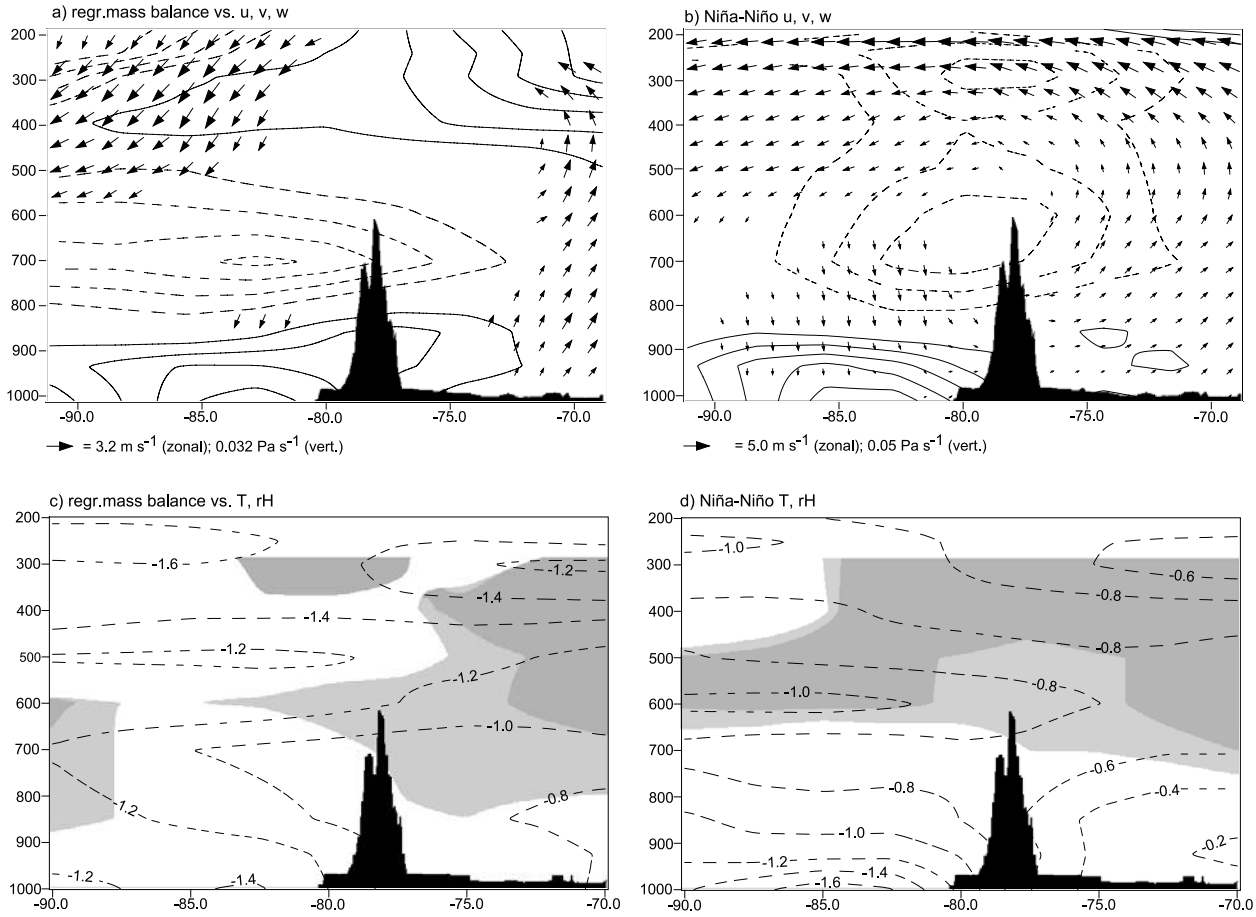

Figure 14. (a) Antizana mass balance anomalies regressed upon three-dimensional wind field in a pressure-longitude cross section along the equator from 90°–70°W between January 1995 and December 2002. Wind vectors indicate zonal and omega vertical velocity. Wind anomalies are only shown if either zonal or vertical velocity component is significantly correlated with Antizana mass balance time series at $p = 0.05$ level. Scale for vectors is shown below. Meridional wind is indicated by contour lines. Contour interval is 0.25 m s^{-1} per m w.e.; zero-contour is omitted, and negative contours are shown (dashed). Andean topography is indicated (black shading). (b) As in Figure 14a but for La Niña–El Niño composite based on ENSO periods as defined in Table 1. Wind vectors are only shown if either zonal or vertical velocity component is significantly different during La Niña as compared to El Niño based on two-tailed Student's t test (at $p = 0.05$ level). (c) As in Figure 14a except for air temperature (°C per m w.e.) and relative humidity (% per m w.e.). Air temperature is indicated by contour lines. Contour interval is 0.2°C; negative contours are shown (dashed). Relative humidity is only shown where correlation with Antizana mass balance time series is significant at $p = 0.05$ and anomalies are >4% per m w.e. (>6% per m w.e.) indicated in light (dark) gray shading. Note that relative humidity analysis extends only to 300 hPa. (d) As in Figure 14b except for air temperature (°C) and relative humidity (%). Scaling is as in Figure 14c. Relative humidity is only shown where it is significantly different during La Niña as compared to El Niño based on two-tailed Student's t test (at $p = 0.05$ level) and difference is >4% (>6%) indicated in light (dark) gray shading.

the equinoxes, which at the same time features the highest S_{TOA}, it comes as no surprise that ablation varies the most around April–May and September.

[46] In general, La Niña events are characterized by cold temperatures, high snowfall amounts, and, to a lesser degree, more constant winds and high humidity. These factors combine to increase albedo and sublimation and therefore preclude melting at the glacier surface during La Niña. El Niño periods, on the other hand, are characterized by increased melt rates, caused both by rainfall on the glacier due to higher temperatures as well as by a deficit of precipitation, both of which contribute to lower the albedo over large areas of the glacier. A significant reduction in cloud cover during the equinoxes of El Niño events has an important effect on the amount of incoming shortwave radiation, thereby leading to the highest melt rates around the equinoxes AMS.

[47] This paper focused on mass balance in the ablation zone, because monthly measurements are only available from this lowest part of the glacier, which is particularly

sensitive to climate variability. However, the upper part of the glacier, where accumulation is dominant, plays a large part in the specific net balance, in particular during La Niña periods with increased precipitation. In such a situation, as it occurred in 1999 and 2000, the accumulation area ratio (AAR) can grow up to 80%, and the glacier mass may increase by 400–500 mm w.e.yr^{-1}. In contrast, during El Niño events the strong melting below the ELA combines with the reduced snow accumulation at higher elevations and leads to a reduced AAR (60% and less) and a very negative mass balance (lower than −500 mm w.e.yr^{-1}). Such a situation was observed in 1995, 1997, 1998, 2001, and 2002.

[48] Correlation of the mass balance record with tropical SSTA shows that highest correlations do not occur in near-coastal areas but in the Niño-4 domain (5°N to 5°S, 160°E to 150°W) in the central equatorial Pacific. Lead-lag correlation analyses further indicate that SSTA in the Niño-4 domain lead mass balance anomalies by 3 months, consistent with the known delayed atmospheric response to ENSO forcing. This lag between tropical Pacific SSTA and atmospheric response aloft the Ecuadorian Andes explains why the largest differences in mass balance between the two phases of ENSO occur from February to May. Both La Niña and El Niño tend to peak in boreal winter (between November and February). Hence the largest impact near Antizana occurs with a 3-month delay around February–May. Indeed this is the time when temperature anomalies between the two phases are largest in the Andes of Ecuador. This delayed ENSO impact has further ramifications as the largest temperature departures coincide with the April–May rainy season, which will further enhance mass balance anomalies due to increased precipitation associated with La Niña (decreased precipitation during El Niño) and the associated changes of the glacier albedo.

[49] The high sensitivity of Antizana 15 mass balance toward ENSO and the fact that the glacier has responded very rapidly to positive or negative mass balance changes in the past make tropical Pacific SST the single most important variable in predicting the future behavior of this glacier. In the outer tropics the seasonal dependence and the mechanisms linking ENSO with glacier mass balance are different, but the strong dependence on tropical Pacific SST with negative mass balance during El Niño and a positive balance during La Niña remains the same. Hence the few glaciers that have been monitored for several years throughout the tropical Andes all indicate a strong dependence on climate variability and change in the tropical Pacific domain. Future changes in the sign, strength, and frequency of ENSO as well as decadal to secular changes in tropical Pacific SST might therefore have major ramifications for the future extent of Andean glaciers.

[50] The 8-year record analyzed in this paper is obviously too short to capture the full envelope of long-term climate variability in the Andes of Ecuador. In addition, much of the ENSO variability in the time period 1995–2002 was dominated by the very strong and unusual 1997/1998 El Niño. Although our results indicate that mass balance on Antizana was not strongly biased by this event, the results presented in this paper have to be interpreted cautiously and should be viewed as a first step toward a better understanding of ENSO-related mass balance variability of inner tropical glaciers. Continued monitoring and longer records, covering additional ENSO events, will be required to verify the significance and accuracy of our conclusions.

[51] **Acknowledgments.** We are grateful for the helpful and detailed comments by Patricio Aceituno, Bryan Mark, and an anonymous reviewer, which allowed us to substantially improve the quality of this manuscript. NCEP-NCAR reanalysis, NOAA Optimum Interpolation (OI) SST V2, CMAP precipitation, and NOAA interpolated OLR data were all provided by the NOAA CIRES Climate Diagnostics Center.

References

Aceituno, P., and A. Montecinos (1993), Circulation anomalies associated with dry and wet periods in the South American Altiplano, *Proc. Fourth Int. Conf. South. Hemisphere Meteorol. Oceanogr., Am. Meteorol. Soc.*, 330–331.

Bendix, J. (2000), Precipitation dynamics in Ecuador and northern Peru during the 1991/92 El Niño: A remote sensing perspective, *Int. J. Remote Sens.*, *21*(3), 533–548.

Bendix, J., S. Gaemmerler, C. Reudenbach, and A. Bendix (2003), A case study of rainfall dynamics during El Niño/La Niña 1997/99 in Ecuador and surrounding areas as inferred from GOES-8 and TRMM-PR observations, *Erdkunde*, *57*(2), 81–93.

Bontron, G., B. Francou, B. Cáceres, L. Maisincho, E. Ayabaca, A. de la Cruz, R. Chango, L. A. Garzón, and D. Neubert (1999), *Glaciar 15 del Antizana (Ecuador). Mediciones Glaciológicas, Hidrométricas, Meteorológicas y Topográficas (Años 1997 y 1998)*, 142 pp., Inst. de Invest. para el Desarrollo, Quito.

Cáceres, B., L. Maisincho, J. D. Taupin, P. Tachker, J. P. Chazarin, B. Francou, and V. Favier (2002), *El Glaciar 15 del Antizana (Ecuador). Balance de Masa, Topografía, Meteorología, Hidrología y Balance de Energía (Año 2001)*, 100 pp., Inst. de Invest. para el Desarrollo, Quito.

Enfield, D. B., and A. M. Mestas-Nuñez (1999), Multiscale variabilities in global sea surface temperatures and their relationship with tropospheric climate patterns, *J. Clim.*, *12*, 2719–2733.

Favier, V., P. Wagnon, J.-P. Chazarin, L. Maisincho, and A. Coudrain (2004), One-year measurements of surface heat budget on the ablation zone of Antizana Glacier 15, Ecuadorian Andes, *J. Geophys. Res.*, *109*, D18105, doi:10.1029/2003JD004359.

Francou, B., P. Ribstein, H. Sémiond, C. Portocarrero, and A. Rodriguez (1995a), Balance de glaciares y clima en Bolivia y Perú. Impactos de los eventos ENSO, *Bull. Inst. Fr. études andines*, *24*(3), 643–654.

Francou, B., P. Ribstein, E. Tiriau, and R. Saravia (1995b), Monthly balance and water discharge on an inter tropical glacier. The Zongo glacier, Cordillera Real, Bolivia, 16°S, *J. Glaciol.*, *42*(137), 61–67.

Francou, B., E. Ramirez, B. Cáceres, and J. Mendoza (2000), Glacier evolution in the tropical Andes during the last decades of the 20th century. Chacaltaya, Bolivia, and Antizana, Ecuador, *Ambio*, *29*(7), 416–422.

Francou, B., M. Vuille, P. Wagnon, J. Mendoza, and J.-E. Sicart (2003), Tropical climate change recorded by a glacier in the central Andes during the last decades of the twentieth century: Chacaltaya, Bolivia, 16°S, *J. Geophys. Res.*, *108*(D5), 4154, doi:10.1029/2002JD002959.

Garreaud, R., and P. Aceituno (2001), Interannual rainfall variability over the South American Altiplano, *J. Clim.*, *14*, 2779–2789.

Garreaud, R. D., and D. S. Battisti (1999), Interannual (ENSO) and interdecadal (ENSO-like) variability in the Southern Hemisphere tropospheric circulation, *J. Clim.*, *12*, 2113–2123.

Garreaud, R., M. Vuille, and A. Clement (2003), The climate of the Altiplano: Observed current conditions and mechanisms of past changes, *Palaeogeogr. Palaeoclimatol. Palaeoecol.*, *194*, 5–22.

Hastenrath, S. (1981), *The Glaciation of the Ecuadorian Andes*, 173 pp., Balkema, Rotterdam, Netherlands.

Kalnay, E., et al. (1996), The NCEP/NCAR 40-year reanalysis project, *Bull. Am. Meteorol. Soc.*, *77*(3), 437–471.

Kaser, G., and H. A. Osmaston (2002), *Tropical Glaciers*, 228 pp., Cambridge Univ. Press, New York.

Kousky, V. E., and M. T. Kayano (1994), Principal modes of outgoing longwave radiation and 250 mb circulation for the South American sector, *J. Clim.*, *7*, 1131–1143.

Kumar, A., and M. P. Hoerling (2003), The nature and causes for the delayed atmospheric response to El Niño, *J. Clim.*, *16*, 1391–1403.

Liebmann, B., and C. A. Smith (1996), Description of a complete (interpolated) outgoing longwave radiation dataset, *Bull. Am. Meteorol. Soc.*, *77*(6), 1275–1277.

Liebmann, B., J. A. Marengo, J. D. Glick, V. E. Kousky, I. C. Wainer, and O. Massambani (1998), A comparison of rainfall, outgoing longwave radiation and divergence over the Amazon basin, *J. Clim.*, *11*, 2898–2909.

Oke, T. R. (1987), *Boundary Layer Climates*, 2nd ed., 435 pp., Routledge, New York.

Reynolds, R. W., N. A. Rayner, T. M. Smith, D. C. Stokes, and W. Q. Wang (2002), An improved in situ and satellite SST analysis for climate, *J. Clim.*, *15*, 1609–1625.

Ribstein, P., B. Francou, E. Tiriau, and R. Saravia (1995), Tropical climate and glacier hydrology. A case study in Bolivia, *J. Hydrol.*, *165*, 221–234.

Rossel, F., R. Mejía, G. Ontaneda, R. Pombosa, J. Roura, P. Le Goulven, E. Cadier, and R. Calvez (1998), Régionalisation de l'influence du El Niño sur les précipitations de l'Equateur, *Bull. Inst. Fr. études andines*, *27*(3), 643–654.

Sicart, J. E. (2002), Contribution à l'étude des flux d'énergie, du bilan de masse et du débit de fonte d'un glacier tropical: Le Zongo, Bolivie, Ph.D. thesis, 330 pp., Univ. de Paris, Paris.

Trenberth, K. (1997), The definition of El Niño, *Bull. Am. Meteorol. Soc.*, *78*(12), 2771–2777.

Villacis, M. J. (2001), *Influencia de El Niño-Oscilación del Sur Sobre la Precipitación en los Andes Centrales del Ecuador, Tesis de Grado*, 199 pp., Esc. Pol. Nac., Quito, Ecuador.

Vuille, M. (1999), Atmospheric circulation over the Bolivian Altiplano during dry and wet periods and extreme phases of the Southern Oscillation, *Int. J. Climatol.*, *19*, 1579–1600.

Vuille, M., and R. S. Bradley (2000), Mean annual temperature trends and their vertical structure in the tropical Andes, *Geophys. Res. Lett.*, *27*, 3885–3888.

Vuille, M., R. S. Bradley, and F. Keimig (2000a), Interannual climate variability in the central Andes and its relation to tropical Pacific and Atlantic forcing, *J. Geophys. Res.*, *105*, 12,447–12,460.

Vuille, M., R. S. Bradley, and F. Keimig (2000b), Climatic variability in the Andes of Ecuador and its relation to tropical Pacific and Atlantic sea surface temperature anomalies, *J. Clim.*, *13*, 2520–2535.

Vuille, M., R. S. Bradley, M. Werner, and F. Keimig (2003), 20th century climate change in the tropical Andes: Observations and model results, *Clim. Change*, *59*(1–2), 75–99.

Wagnon, P., P. Ribstein, B. Francou, and B. Pouyaud (1999), Annual cycle of energy balance of Zongo glacier, Cordillera Real, Bolivia, *J. Geophys. Res.*, *104*, 3907–3923.

Wagnon, P., P. Ribstein, B. Francou, and J. E. Sicart (2001), Anomalous heat and mass budget of Zongo glacier, Bolivia, during the 1997–98 El Niño year, *J. Glaciol.*, *47*(156), 21–28.

World Glacier Monitoring Service (2003), *Glacier Mass Balance Bulletin (2000–2001)*, vol. 7, edited by W. Haeberli, R. Frauenfelder, and M. Hoelzle, World Meteorol. Organ., Geneva.

Xie, P., and P. A. Arkin (1997), Global precipitation: A 17-year monthly analysis based on gauge observations, satellite estimates, and numerical model outputs, *Bull. Am. Meteorol. Soc.*, *78*(11), 2539–2558.

Yulaeva, E., and J. M. Wallace (1994), The signature of ENSO in global temperature and precipitation fields derived from the microwave sounding unit, *J. Clim.*, *7*, 1719–1736.

B. Cáceres, Instituto Nacional de Meteorología e Hidrología (INAMHI), Ap. Postal 1712857, Quito, Ecuador. (bolivar@inamhi.gov)

V. Favier, UR Great Ice, Institut de Recherche pour le Developpement, Maison des Sciences de l'Eau, 300 Av. Emile, Jeanbrau, Montpellier, F-34095 France. (favier@msem.univ-montp2.fr)

B. Francou, Institut de Recherche pour le Developpement, Laboratoire de Glaciologie et de Géophysique de l'Environnement, Domaine Universitaire - BP. 96, St. Martin d'Hères, F-38402 France. (francou@glaciog.ujf-grenoble.fr)

M. Vuille, Climate System Research Center, Department of Geosciences, University of Massachusetts, Amherst, MA 01003-5820, USA. (mathias@geo.umass.edu)